Kolmogorov Turbulence in Low-Temperature Superflows

C. Nore,[1] M. Abid,[2] and M. E. Brachet[1]
[1]*Laboratoire de Physique Statistique de l'Ecole Normale Supérieure, associé au CNRS et aux Universités Paris 6 et 7, 24 Rue Lhomond, 75231 Paris Cedex 05, France*
[2]*Institut de Recherche sur les Phénomènes Hors Equilibre, UMR CNRS et Université d'Aix-Marseille I, service 252, Centre St-Jérôme, 13397 Marseille Cedex 20, France*
(Received 11 December 1996)

Low-temperature decaying superfluid turbulence is studied using the nonlinear Schrödinger equation in the geometry of the Taylor-Green (TG) vortex flow with resolutions up to 512^3. The rate of (irreversible) kinetic energy transfer in the superfluid TG vortex is found to be comparable to that of the viscous TG vortex. At the moment of maximum dissipation, the energy spectrum of the superflow has an inertial range compatible with Kolmogorov's scaling. Physical-space visualizations show that the vorticity dynamics of the superflow is similar to that of the viscous flow, including vortex reconnection. The implications to experiments in low-temperature helium are discussed. [S0031-9007(97)03046-9]

PACS numbers: 67.40.Vs, 47.37.+q, 67.40.Hf

Superfluid flows are described mathematically in terms of Landau's two-fluid model [1]. When both normal fluid and superfluid vortices are present, their interaction, called "mutual friction," must be taken into account as pioneered by Schwarz [2]. At temperatures low enough for the normal fluid to be negligible (in practice below $T = 1$ K for helium at normal pressure), an alternative mathematical description is given by the nonlinear Schrödinger equation (NLSE), sometimes also called the Gross-Pitaevskii equation [3,4]. The NLSE reads

$$\partial_t \psi = (ic/\sqrt{2}\,\xi)(\psi - |\psi|^2\psi + \xi^2\nabla^2\psi). \qquad (1)$$

The complex wave field ψ is related to the superflow's density ρ and velocity v by Madelung's transformation $\rho = |\psi|^2$, $\rho v_j = (ic\xi/\sqrt{2})(\psi\partial_j\overline{\psi} - \overline{\psi}\partial_j\psi)$, where ξ is the so-called "coherence length" and c is the velocity of sound (when the mean density $\rho_0 = 1$ [5]). The superflow is irrotational, except near the nodal lines of ψ which are known to follow Eulerian dynamics [6,7]. These topological defects correspond to the superfluid vortices that appear naturally, with the correct velocity circulation, in this model [8].

The basic goal of the present Letter is to qualify the degree of analogy between turbulence in low-temperature superfluids and incompressible viscous fluids. We will do this by comparing numerical simulations of NLSE with existing numerical simulations of the Navier-Stokes equations, in particular the Taylor-Green (TG) vortex [9]. The TG vortex is the solution of the Navier-Stokes equations with initial velocity field $\mathbf{v}^{\mathrm{TG}} = (\sin(x)\cos(y)\cos(z), -\cos(x)\sin(y)\cos(z), 0)$. This flow is well documented in the literature [10–12]. It admits symmetries that are used to speed up computations: rotation by π about the axis $(x = z = \pi/2)$, $(y = z = \pi/2)$, and $(x = y = \pi/2)$, and reflection symmetry with respect to the planes $x = 0, \pi$, $y = 0, \pi$, $z = 0, \pi$. The velocity is parallel to these planes which form the sides of the *impermeable box* which confines the flow. The TG flow is related to an experimentally studied swirling flow [13–15]. The relation between the experimental flow and the TG vortex is a similarity in overall geometry [13]: a shear layer between two counterrotating eddies. The TG vortex, however, is periodic with free-slip boundaries while the experimental flow is contained inside a tank between two counterrotating disks.

We now show how to construct a vortex array whose NLSE dynamics mimics the vortex dynamics of the large scale flow $\mathbf{v}^{\mathrm{TG}}$. The first step of our method is based on a global Clebsch representation of $\mathbf{v}^{\mathrm{TG}}$ and the second step minimizes the emission of acoustic waves [16].

The Clebsch potentials $\lambda(x, y, z) = \cos(x)\sqrt{2|\cos(z)|}$, $\mu(x, y, z) = \cos(y)\sqrt{2|\cos(z)|}\,\mathrm{sgn}(\cos(z))$ (where sgn gives the sign of its argument) correspond to the TG flow in the sense that $\nabla\mathbf{v}^{\mathrm{TG}} = \nabla\lambda \times \nabla\mu$. The complex field ψ_c, corresponding to the large scale TG flow circulation, is given by $\psi_c(x, y, z) = (\psi_4(\lambda, \mu))^{[\gamma_d/4]}$ with $\gamma_d = 2\sqrt{2}/(\pi c\xi)$ ([ ] is the integer part of a real) and

$$\psi_4(\lambda, \mu) = \psi_e(\lambda - 1/\sqrt{2}, \mu)\psi_e(\lambda, \mu - 1/\sqrt{2}) \times \psi_e(\lambda + 1/\sqrt{2}, \mu)\psi_e(\lambda, \mu + 1/\sqrt{2}),$$

where $\psi_e(\lambda, \mu) = (\lambda + i\mu)\tanh(\sqrt{\lambda^2 + \mu^2}/\sqrt{2}\xi)/\sqrt{\lambda^2 + \mu^2}$.

The second step of our procedure consists of integrating to convergence the advective real Ginzburg-Landau equation (ARGLE):

$$\partial_t\psi = (c/\sqrt{2}\xi)(\psi - |\psi|^2\psi + \xi^2\nabla^2\psi) - i\mathbf{v}^{\mathrm{TG}}\cdot\nabla\psi - [(\mathbf{v}^{\mathrm{TG}})^2/2\sqrt{2}\,c\xi]\psi, \qquad (2)$$

with initial data $\psi = \psi_c$. This amounts to minimizing the functional

$$\mathcal{F} = (c/\sqrt{2}\,\xi)\int d^3\vec{x}\,[-|\psi|^2 + |\psi|^4/2 + \xi^2|\nabla\psi - (i\mathbf{v}^{\mathrm{TG}}/\sqrt{2}\,c\xi)\psi|^2]. \qquad (3)$$

It is shown in [17] that replacing $\mathbf{v}^{\mathrm{TG}}$ by a constant vector yields as a minimum of (3) a boosted straight vortex line that is an exact radiationless solution of (1).

 0031-9007/97/78(20)/3896(4)$10.00

Minimizing (3) with the space-dependent $\mathbf{v}^{\mathrm{TG}}$ applies to the vortex lines a local Galilean boost with velocity $\mathbf{v}^{\mathrm{TG}}$. The TG symmetries can be used to expand $\psi(x, y, z, t) = \sum_{m=0}^{N/2} \sum_{n=0}^{N/2} \sum_{p=0}^{N/2} \hat{\psi}(m, n, p, t) \cos mx \cos ny \times \cos pz$ where N is the resolution and $\hat{\psi}(m, n, p, t) = 0$, unless m, n, p are either all even or all odd integers. Implementing this expansion in a pseudospectral code yields a saving of a factor 64 in computational time and memory size when compared to general Fourier expansions. The ARGLE converged periodic vortex array obtained in this manner is displayed on Fig. 1. Note that the radius of curvature of the vortex lines is large compared to their radius.

The total energy of the vortex array, conserved by NLSE dynamics, can be decomposed into three parts $E_{\mathrm{tot}} = (1/2\pi)^3 \int d^3x \, (\mathcal{E}_{\mathrm{kin}} + \mathcal{E}_{\mathrm{int}} + \mathcal{E}_q)$, with kinetic energy $\mathcal{E}_{\mathrm{kin}} = \frac{1}{2} \rho v_j v_j$, internal energy $\mathcal{E}_{\mathrm{int}} = (c^2/2)(\rho - 1)^2$, and quantum energy $\mathcal{E}_q = c^2 \xi^2 (\partial_j \sqrt{\rho})^2$. Each of these parts can be defined as the integral of the square of a field, for example, $\mathcal{E}_{\mathrm{kin}} = \frac{1}{2} (\sqrt{\rho} v_j)^2$. Using Parseval's theorem, the angle-averaged kinetic energy spectrum is defined as

$$E_{\mathrm{kin}}(k) = \frac{1}{2} \int k^2 \sin\theta \, d\theta \, d\phi \times \left| \frac{1}{(2\pi)^3} \int d^3r \, e^{i r_j k_j} \sqrt{\rho} \, v_j \right|^2 ,$$

which satisfies $E_{\mathrm{kin}} = 1/(2\pi)^3 \int d^3x \, \mathcal{E}_{\mathrm{kin}} = \int_0^\infty dk \times E_{\mathrm{kin}}(k)$. The angle-average is performed by summing over shells in Fourier space. A mode (m, n, p) belongs to the shell $k = [\sqrt{m^2 + n^2 + p^2} + 1/2]$. E_{kin} is further decomposed into compressible E_{kin}^c and incompressible E_{kin}^i parts, using $\sqrt{\rho} v_j = (\sqrt{\rho} v_j)^c + (\sqrt{\rho} v_j)^i$ with $\nabla (\sqrt{\rho} v_j)^i = 0$. This simple decomposition has the advantage over the more conventional one, $\sqrt{\rho} v_j = \sqrt{\rho} (v_j)^c + \sqrt{\rho} (v_j)^i$, of not involving a mixed compressible-incompressible energy spectrum. We have checked that both decompositions give the same behavior for $E_{\mathrm{kin}}^i(k)$ in the runs presented below.

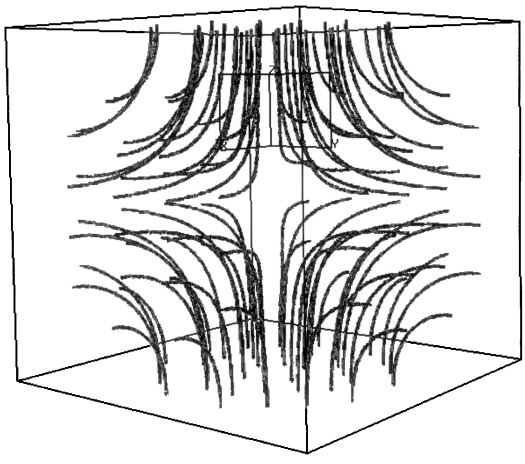

FIG. 1. Three-dimensional visualization of the vector field $\nabla \times (\rho \vec{v})$ for the Taylor-Green flow at time $t = 0$ with coherence length $\xi = 0.1/(8\sqrt{2})$, sound velocity $c = 2$, and resolution $N = 512$ in the impermeable box $[0, \pi] \times [0, \pi] \times [0, \pi]$. The visualization is obtained by drawing the 30 000 vectors of highest norm.

An exact solution of NLSE, describing a 2D axisymmetric vortex, is given by $\psi^{\mathrm{vort}}(r) = \sqrt{\rho(r)} \exp(im\varphi)$, $m = \pm 1$, where (r, φ) are polar coordinates. The vortex profile $\sqrt{\rho(r)} \sim r$ as $r \to 0$ and $\sqrt{\rho(r)} = 1 + O(r^{-2})$ for $r \to \infty$. It can be computed numerically using mapped Chebychev polynomials expansions and an appropriate functional [17]. The corresponding velocity field is azimuthal and is given by $v(r) = \sqrt{2} c \xi / r$. Using the expansion for $\sqrt{\rho(r)}$, the 2D angle-averaged spectrum of $\sqrt{\rho} v_j$ can then be computed with the formula $E_{\mathrm{kin}}^{\mathrm{vort}}(k) = (c^2 \xi^2 / 2\pi k) [\int_0^\infty dr \, J_0(kr) \partial_r \sqrt{\rho}]^2$, where J_0 is the zeroth order Bessel function. It is shown in [17] that, when a 3D isolated vortex line is almost straight, the 3D angle-averaged spectrum of the line is given by $E_{\mathrm{kin}}^{\mathrm{line}}(k) = (l/2\pi) E_{\mathrm{kin}}^{\mathrm{vort}}(k)$, where l is the length of the line.

Indeed, the incompressible kinetic energy spectrum $E_{\mathrm{kin}}^i(k)$ of the ARGLE converged vortex array of Fig. 1 displayed on Fig. 2(a) is well represented, at large k, by an isolated line spectrum $E_{\mathrm{kin}}^{\mathrm{line}}(k)$ with total vortex length given by $l/2\pi = 175$. In contrast, the small wave number region cannot be represented by $E_{\mathrm{kin}}^{\mathrm{line}}(k)$. This stems from the average separation distance between the vortex lines in Fig. 1. Calling this distance $d_{\mathrm{bump}} \sim k_{\mathrm{bump}}^{-1} = 1/16$, the wave number range between the large-scale wave number $k = 2$ and the characteristic separation wave number k_{bump} can be explained by

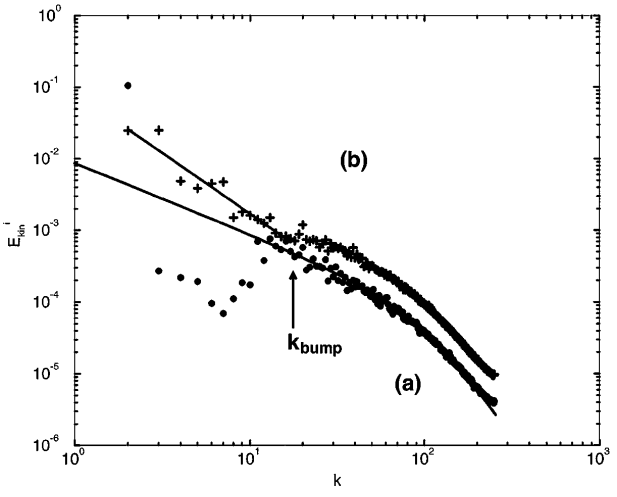

FIG. 2. Plot of the incompressible kinetic energy spectrum, $E_{\mathrm{kin}}^i(k)$. The bottom curve (a) (circles) corresponds to time $t = 0$ (same conditions as in Fig. 1). The spectrum of a single axisymmetric 2D vortex multiplied by $(l/2\pi) = 175$ is shown as the bottom solid line. The top curve (b) (plusses) corresponds to time $t = 5.5$. A least-square fit over the interval $2 \le k \le 16$ with a power law $E_{\mathrm{kin}}^i(k) = Ak^{-n}$ gives $n = 1.70$ (top solid line).

interference effects. Because of constructive interference, the energy spectrum at $k = 2$ has a value close to its corresponding value in TG viscous flow (namely 0.125), which is much above the value of $E^{\text{line}}_{\text{kin}}(k = 2)$. In contrast, for $2 < k \leq k_{\text{bump}}$, destructive interference decreases $E^{i}_{\text{kin}}(k)$ below $E^{\text{line}}_{\text{kin}}(k)$. This spectral situation can be understood by analogy with the reproduction of a grey scale picture using black dots. The small wave number spectrum of the reproduction will be that of the original picture, while the large wave number spectrum will be that of the individual dots. Here the dots are vortex lines and the picture is $\mathbf{v}^{\text{TG}}$.

The evolution in time via NLSE (1) of the incompressible kinetic energy is shown in Fig. 3 for various values of ξ, the resolution N being adjusted to maintain accuracy. The main quantitative result of this Letter is the remarkable agreement of the energy dissipation rate $-dE^{i}_{\text{kin}}/dt$ with the corresponding data in the incompressible viscous TG flow. Both the moment $t_{\text{max}} \sim 5$–10 of maximum energy dissipation (the inflection point of Fig. 3) and its value $\epsilon(t_{\text{max}}) \sim 10^{-2}$ at that moment are in quantitative agreement with the viscous data [10,18]. Furthermore, both t_{max} and $\epsilon(t_{\text{max}})$ depend weakly on ξ. This is remarkably similar to the weak dependence of the corresponding viscous dissipation in the limit of small viscosity. This weak dependence is considered a hallmark of numerical evidence for a Kolmogorov regime in decaying turbulence [18].

Another important quantity studied in viscous decaying turbulence is the scaling of the kinetic energy spectrum during time evolution and, especially, at the moment of maximum energy dissipation, where a $k^{-5/3}$ range can be observed [10]. Figure 2(b) shows the energy spectrum at $t = 5.5$. A least-square fit over the interval $2 \leq k \leq 16$ with a power law $E^{i}_{\text{kin}}(k) = Ak^{-n}$ gives $n = 1.70$ (solid line). For $5 < t < 8$, a similar fit gives $n = 1.6 \pm 0.2$ (data not shown). Although uncertain, the value of n is compatible with Kolmogorov's $\frac{5}{3}$ value. The time evolution of $l/2\pi$ obtained by representing the high-k region of E^{i}_{kin} by a line spectrum $E^{\text{line}}_{\text{kin}}$ is displayed in Fig. 3. The length saturates beyond t_{max} at roughly three times its $t = 0$ value. Although the volume occupied by the vortices has increased, it remains a small fraction $l\pi\xi^2/(2\pi)^3 \sim 0.4\%$ of the total volume of the box. The computations were performed with $c = 2$ corresponding to a *root-mean-square* Mach number $M_{\text{rms}} \equiv |\mathbf{v}^{\text{TG}}_{\text{rms}}|/c = 0.25$. As it is very costly to decrease M_{rms}, we checked [17] that compressible effects were nondominant at this value of M_{rms}. In particular, E^{i}_{kin} is well above the other energy spectra throughout the run for $k < k_{\text{bump}}$.

It is known [19] that NLSE vortex lines can reconnect. The vortex lines are visualized in physical space in Figs. 4 and 5 at times $t = 4$ and $t = 8$. At $t = 4$, no reconnection has yet taken place while a complex vortex tangle is present at $t = 8$. Detailed visualizations (data not shown) demonstrate that reconnections occur for $t > 5$. Note that in the viscous TG vortex reconnection also sets in for $t > 5$.

As seen above, the spectral behavior of NLSE can be compared to viscous turbulence only for $k \leq k_{\text{bump}} \sim d^{-1}_{\text{bump}}$, where d_{bump} is the average distance between neighboring vortices. We now estimate the scaling of k_{bump} in terms of the flow integral scale l_0 and velocity u_0 and of the velocity of sound c and coherence length ξ. The number n_d of vortex lines crossing a large-scale l_0^2 area is given by the ratio of the circulation $l_0 u_0$ to the quantum of circulation $\Gamma = 4\pi c\xi/\sqrt{2}$, i.e., $n_d \sim l_0 u_0/c\xi$. Assuming that the vortices are uniformly

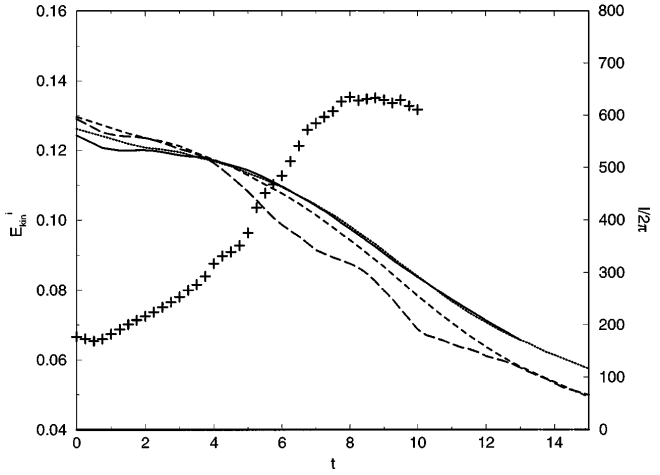

FIG. 3. Total incompressible kinetic energy E^{i}_{kin} plotted versus time for $\xi = 0.1/(2\sqrt{2})$ and resolution $N = 128$ (long-dash line); $\xi = 0.1/(4\sqrt{2})$, $N = 256$ (dash); $\xi = 0.1/(6.25\sqrt{2})$, $N = 400$ (dot); and $\xi = 0.1/(8\sqrt{2})$, $N = 512$ (solid line). All runs are realized with $c = 2$. The evolution of the total vortex filament length divided by 2π (crosses) for the $N = 512$ run is also shown (scale given on the right y axis).

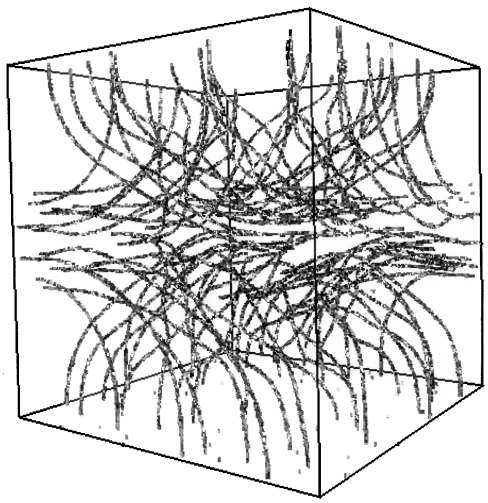

FIG. 4. Same visualization as in Fig. 1, but at time $t = 4$.

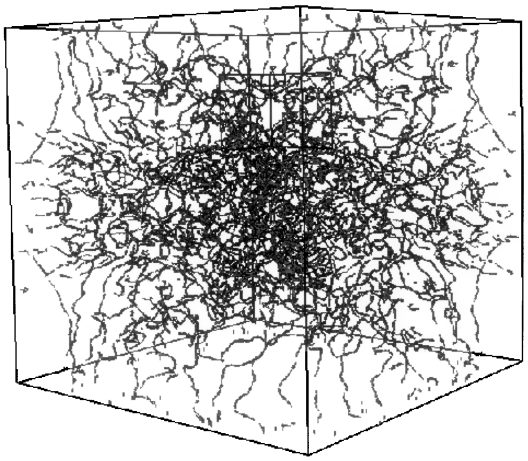

FIG. 5. Same visualization as in Fig. 1, but at time $t = 8$.

spread over the large scale area gives $n_d \sim l_0^2/d_{\text{bump}}^2$. Equating these two evaluations of n_d yields $d_{\text{bump}} \sim l_0\sqrt{(c\xi)/(l_0 u_0)}$.

In the case of helium, the viscosity at the critical point ($T = 5.174$ K, $P = 2.210^5$ Pa) is $\nu_{cp} = 0.27 \times 10^{-7}\ \text{m}^2\,\text{s}^{-1}$ while the quantum of circulation, $\Gamma = h/m_{\text{He}}$ has the value $0.99 \times 10^{-7}\ \text{m}^2\,\text{s}^{-1}$. Thus, $4\nu_{cp} \sim \Gamma$ and $d_{\text{bump}} \sim l_0/\sqrt{R_{cp}} \sim l_\lambda$, where R_{cp} is the integral scale Reynolds number at the critical point and l_λ the Taylor microscale. The value of d_{bump} in a superfluid helium experiment at $T = 1$ K is thus of the same order as the Taylor microscale in the same experimental set-up run with viscous helium at the critical point.

An experiment corresponding to the numerical results of the present Letter must be performed at a temperature low enough for the normal component of the flow to be neglected. In this regime, second sound attenuation measurements cannot be performed. Preliminary measurements (J. Maurer, private communication) in the swirling flow of Ref. [14] did not seem to show any significant change in energy dissipation for temperatures as low as 1.6 K where the normal fluid and the superfluid are in the same proportion. It would be interesting to know if such behavior persists at $T < 1$ K. In viscous turbulence, it is well known that Kolmogorov's theory is only approximate since it neglects intermittency [18]. Inertial range "intermittency corrections" are measured [14,20,21] on velocimetry data by monitoring the scaling of high order moments of velocity increments. If the corresponding superfluid quantities could be measured experimentally below $T = 1$ K by an as-yet-to-be-developed velocimetry probe, significant differences might appear.

In summary, turbulent solutions of NLSE—and thus low-temperature superfluid turbulence—approximately obey Kolmogorov's scaling. A question, open to experimental investigations, is to know the exact limits of this analogy between superfluid and viscous turbulence. Some important experimental properties, such as Kolmogorov's scaling, still evade first principle derivation from the Navier-Stokes equations [18]. These hard problems may be easier to solve, when the analogy is valid, using the NLSE rather than the Navier-Stokes equations.

Computations were performed on the C94-C98 of the Institut du Développement et des Ressources en Informatique Scientifique. We would like to thank L. Tuckerman for her helpful discussions on this work.

[1] L. Landau and E. Lifchitz, *Fluid Mechanics* (Pergamon Press, Oxford, 1980).
[2] K. W. Schwarz, Phys. Rev. B **31**, 5782 (1985).
[3] E. P. Gross, J. Math. Phys. **4**, 195 (1963).
[4] V. L. Ginzburg and L. P. Pitaevskii, Sov. Phys. JETP **34**, 858 (1958).
[5] R. J. Donnelly, *Quantized Vortices in Helium II* (Cambridge University Press, Cambridge, England, 1991).
[6] J. C. Neu, Physica (Amsterdam) **43D**, 385 (1990).
[7] F. Lund, Phys. Lett. A **159**, 245 (1991).
[8] P. Nozières and D. Pines, *The Theory of Quantum Liquids* (Addison-Wesley, New York, 1990).
[9] G. I. Taylor and A. E. Green, Proc. R. Soc. London A, **158**, 499 (1937).
[10] M. E. Brachet, D. I. Meiron, S. A. Orszag, G. Nickel, R. H. Morf, and U. Frisch, J. Fluid Mech. **130**, 411 (1983).
[11] M. Brachet, C. R. Acad. Sci. Ser. 2 **311**, 775 (1990).
[12] J. Domaradzki, W. Liu, and M. Brachet, Phys. Fluids A **5**, 1747 (1993).
[13] S. Douady, Y. Couder, and M. E. Brachet, Phys. Rev. Lett. **67**, 983 (1991).
[14] G. Zocchi, P. Tabeling, J. Maurer, and H. Willaime, Phys. Rev. E **50**, 3693 (1994).
[15] S. Fauve, C. Laroche, and B. Castaing, J. Phys. II (France) **3**, 271 (1993).
[16] C. Nore, M. Abid, and M. Brachet, C. R. Acad. Sci. Ser. 2 **319**, 733 (1994).
[17] C. Nore, M. Abid, and M. Brachet, Phys. Fluids (to be published).
[18] U. Frisch, *Turbulence, the Legacy of A. N. Kolmogorov* (Cambridge University Press, Cambridge, England, 1995).
[19] J. Koplik and H. Levine, Phys. Rev. Lett. **71**, 1375 (1993).
[20] Y. Gagne, E. Hopfinger, and U. Frisch, in *A New Universal Scaling for Fully Developed Turbulence: The Distribution of Velocity Increments*, NATO ASI, Vol. 237, edited by P. Coullet and P. Huerre (Plenum, New York, 1990), p. 315.
[21] F. Belin, P. Tabeling, and H. Willaime, Physica (Amsterdam) **93D**, 52 (1996).